International Journal of Science, Technology and Society
2022; 10(5): 198-216
http://www.sciencepublishinggroup.com/j/ijsts
doi: 10.11648/j.ijsts.20221005.16
ISSN: 2330-7412 (Print); ISSN: 2330-7420 (Online)

Mining Exploration in the Pan-African Province of Damagaram-Mounio (Eastern Niger), Using Termite Mound Geochemistry and High Resolution Airborne Geophysics

Djibo Maiga Abdoul Wahab*, Moussa Konate

Department of Geology, Abdou Moumouni University, Niamey, Niger

Email address:

djibowahab@gmail.com (Djibo Maiga Abdoul Wahab)

*Corresponding author

To cite this article:

Djibo Maiga Abdoul Wahab, Moussa Konate. Mining Exploration in the Pan-African Province of Damagaram-Mounio (Eastern Niger), Using Termite Mound Geochemistry and High Resolution Airborne Geophysics. *International Journal of Science, Technology and Society*. Vol. 10, No. 5, 2022, pp. 198-216. doi: 10.11648/j.ijsts.20221005.16

Received: September 24, 2022; **Accepted**: October 24, 2022; **Published**: October 30, 2022

Abstract: The Damagaram-Mounio region is one of the metallogenic provinces of Niger belonging to the Pan-African Mobile Zone where mining exploration began in 1903. Several exploration missions including geological mapping, hammer prospecting, geochemistry and airborne geophysics have been undertaken. Among others results termite geochemistry conducted between 1984 and 1985 have highlighted interesting targets of several minerals. More recently, from 2007 to 2010, high resolution airborne geophysical surveys, using Mag/Spectro in the Damagaram-Mounio Province, have allowed identification of mining targets, including target EM_1 which covers the southern part of the surveyed area by termite mounds geochemistry. The target EM_1 has also been explored by Mag/EM surveys. This study aims to reinterpret the termite mound geochemistry results in relation with high resolution airborne geophysical survey and satellite imageries data using more recent software dedicated to this purpose. The interpretation of the airborne geophysical data will allow characterizing the magnetic, spectrometric and electromagnetic contexts of the part of the target EM_01 where termite mounds was sampled. In addition, these results of high resolution airborne geophysical surveys will allow interpreting the structures, their orientations but also their spatial continuity to which can be associated the anomal grade values highlighted by the termite geochemistry. Indeed, it is known that termites build their mounds with water and materials that they seek at a depth of several tens of meters underground. In the Damagaram-Mounio Province, termites can only find water in the fracture zones of the Pan-African basement and of the "Younger Granites" Ring Complex.

Keywords: Pan-African Damagaram-Mounio, Gouré, Alkaline Ring Complexes, Termite Mound Geochemistry

1. Introduction

The Pan-African Damagaram-Mounio Province (DMP), located in Southeastern Niger, is part of the Trans-Saharan orogenic belt [13, 15, 17, 20-22]. It represents the southern part of the Trans-Saharan belt on which lie Permo-Cretaceous to Quaternary sediments. On a regional scale, the Pan-African DMP is linked to the Aïr Massif and the Tuareg Shield to the north, and to the Nigeria-Benin Shield to the south.

Several mineral showings and targets have been highlighted following hammer prospecting, geological mapping, rock geochemical prospecting, termite mound prospecting and airborne geophysical prospecting missions [24, 26]. Geological mapping coupled with termite mound geochemistry was carried out between 1984 - 1985 [4, 31] in Mounio area (Gouré complex and central Mounio). The termite geochemistry analyzed fifteen (15) elements including Cu, Pb, Zn, Ag, Ni, Co, Fe, Mn, Mo, Sn, As, Sb, U, Au, Cr.

From 2007 to 2010, a program of airborne geophysical surveys (Mag/Spectro, Mag/EM) was implemented, particularly in Damagaram-Mounio area [23]. Several targets have been identified, including target EM_1 covering the southern part of the termite geochemical survey area (Figure 1).

Previous interpretations, due to the cover of Quaternary sand that constitutes a screen for soil, alluvial and rock

geochemistry on the one hand, and insufficient structural data on the other hand, did not allow mining potential evaluation of the prospect highlighted in the southern part of Mounio.

The purpose of this study is to analyze the results of termite mound geochemistry in relation with the high resolution airborne geophysics results and satellite imagery data. More specifically, it will:

1) Analyze the results of the termite geochemical survey by monovariate and multivariate statistics;
2) Interpret the structures using aeromagnetic geophysical data;
3) Process and interpret satellite imagery to highlight structures;
4) Highlight potassium anomalies along geological structures, possibly associated with hydrothermal processes;
5) Interpret the conductivity of rocks in particular.

2. Geological Framework

The Damagaram-Mounio metallogenic province is part of the Trans-Saharan Mobile Belt. It lies between the Aïr Massif to the North and the Nigerian and Benin shields to the South (Figure 1). The geological framework of Damagaram Mounio is characterized by Paleo- to Neoproterozoic supra-crustal crystalline formations composed of meta-sediments intruded by Paleo to Neoproterozoic calc-alkaline granitoids, and later by Carboniferous to Permian alkaline ring complexes notably Gouré and Zarnouski complexes [5-7, 12]. These ring complexes were exhumed and eroded before being covered by sedimentary rocks during the Cretaceous and Cenozoic periods.

The structural context of the metallogenic province is marked by NE-SW trending and strong dipping geological formations which were affected by N20° and N130° shear zones. The faults are sometimes underlined by decimetric to multi-metric quartz veins.

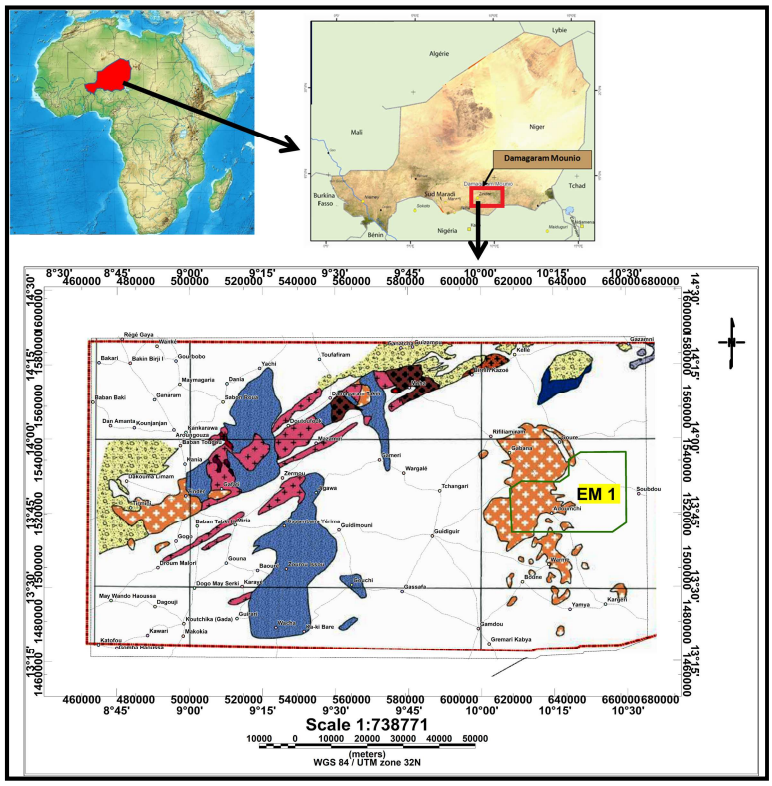

Quaternary dune and alluvium
Late Cretaceous and Continental Terminal (Koutous sandstone)
Alkaline granitic annular complexes
Tyanza fine-grained biotite syenogranite
Birnin Kazoé Biotite granite
High Raffa Schistosity Biotite Granodiorite

Calco-alkaline granite

Dakoussa syenogranite Post-kinematic granite
Moha Monzogranite
Zermou Monzogranite large porphyritic Granite phenocrysts

Basement metasediments

Gazami Polygenic Conglomerate
Biotite-muscovite gneiss
Metaconglomerate, calc-silicate gneiss

Figure 1. *Geology map of the Damagaram-Mounio Province (Black and Liégeois 1991, modified).*

The Target EM_1 covers the southern part of the surveyed area, by termite mound geochemistry. It is located in the Mounio ring complex (Figure 1) and extends over a distance of 43 km from the East to the West and 33 km from the North to the South. The Target EM_1 covers an area of about 1166 km². The termite mound area covered by target EM_1 extends from 12 km NS to 20 km EW, covering an area of 240 km².

This ring complex is essentially characterized by felsic volcanic rocks, initially mapped as rhyolites, felsic breccias and tuffs (Figure 2). It includes also granites and syenites. The central part of the ring complex is occupied by syenite surrounded by a ring of aegirine-riebeckite-goureite microgranites and aegirine-hornblende microgranites [11, 18, 20-22]. These granites are also present in the southern part of the Mounio Ring Complex. These various granites have been mapped from their geophysical characteristics either as syenite-syenogranites or as alkline-hyper alkaline granites.

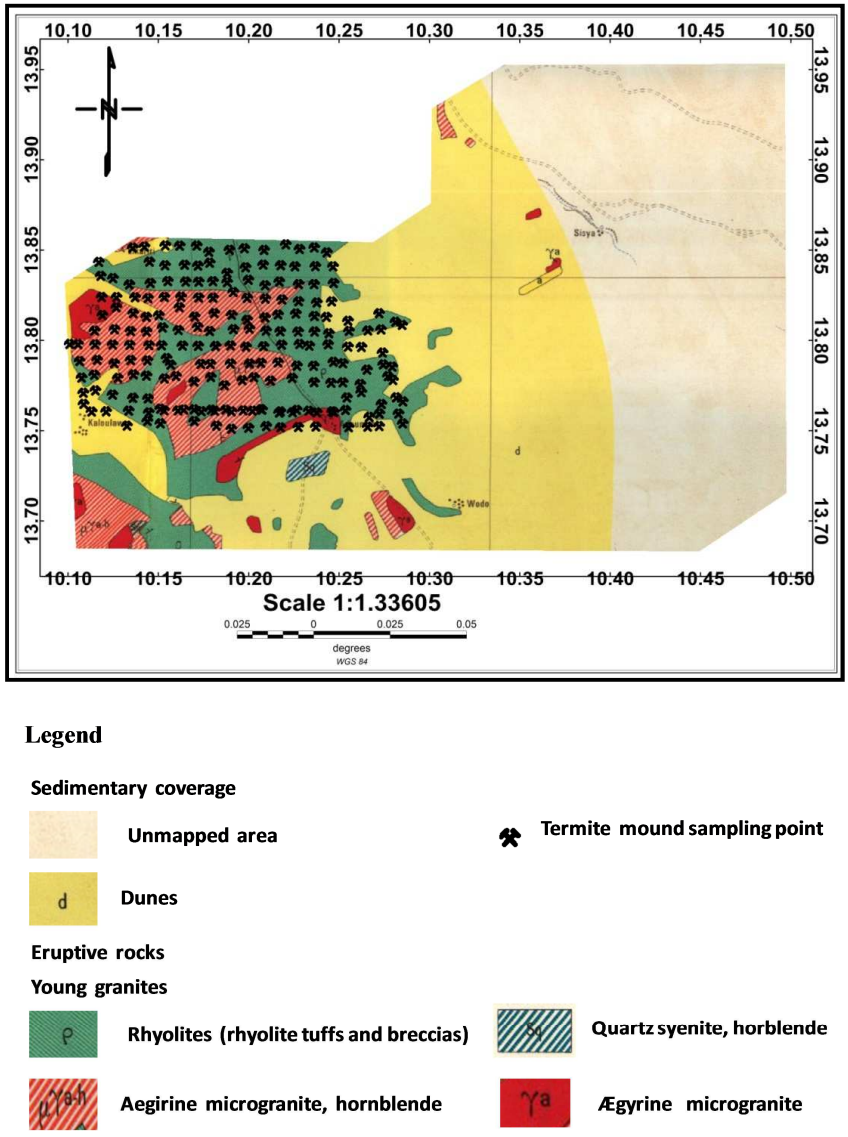

Figure 2. *Geological map of target EM_1 and location of termite mound samples (extracted from the geological map of R. Mignon, 1970).*

3. Methodology

All available data including termite mound geochemistry, airborne geophysical data, satellite imageries and geological data were used. A field mission in the Damagaram-Mounio allowed observations on outcropping rocks. The data will be statistically analyzed and processed before being used for elaboration of geochemical and geophysical anomaly maps and satellite imageries using dedicated software.

3.1. Termite Mound Geochemistry

Two hundred and nine (209) termite mound samples covered by target EM_1 (Cf. Figure 2) out of the six hundred and seventeen (617) termite mounds geochemical survey carried out within the framework of the project " Assistance en recherche minière phase II au Niger " will be processed and reinterpreted [1-3, 25].

3.2. Airborne Geophysics

Mag/Spectro and Mag/EM methods covered the EM_1 target [23]. The aircraft flight lines, oriented N90°, are 250 m apart and the tie lines oriented N180° are 2500 m apart. The helicopter flight lines are 200 m equidistant. The data were sampled at a frequency of 1Hz for magnetometry, per second for aircraft spectrometry and 10Hz for electromagnetism and 1Hz for helicopter magnetometry. Thematic maps including total field, vertical derivative, horizontal derivative, analytical signal, for magnetic data, K, spectrometry, resistivity for electromagnetism will be developed.

3.3. Satellite Imagery

Landsat 7 ETM+ and Landsat 8 data from the seven (7) spectral bands were processed and exploited. The images from the combination of the following bands were produced: bands 3, 2 and 1, band 6, 5, 3, band 7, 4, 1 and the ratios of bands 7/5, 7/4, 5/1.

The maps of iron oxides, clays-minerals and hydrothermal composite were also elaborated and exploited. The exploitation of satellite imageries will be used to interpret faults and lineaments.

3.4. Fractures Analysis

Landsat imagery and geophysical maps will be interpreted manually. Appropriates software were used to interpret the lineaments, the faults and their statistics.

3.5. Geological Reconnaissance Mission

A field trip in Damagaram-Mounio area was carried out, consisting of rock observations and sampling. These field observations made during this reconnaissance mission are used to interpret the geophysical signatures of the rocks in the termite mound area.

3.6. Synthesis of Thematic Results

After the analysis and interpretation of the thematic data, the results were synthesized to produce geochemical anomaly maps and structural interpretations.

4. Results and Discussion

4.1. Geochemical Interpretation

4.1.1. Monovariate Statistical Analysis

The standard statistical analysis of the grade obtained from the geochemical analysis of the termite mounds samples (Table 1)**,** gives the parameters [1-2, 27, 29]. Such as the mean, the standard deviation, the median, the mode, the kurtosis, the coefficient of asymmetry etc....

It appears from this statistic analysis that:

1) the mode is zero (0) for Ag, As, Sb;
2) the highest kurtosis are related to the result of the analysis of the elements Au, As, Cr, Mo, Sb, U. The distribution curves of these elements exhibit sharp profile. This kind of profile is justified for elements with zero modes. The values are close to zero for Ag, Co, Fe and Mn, that are related to their rather flat distribution curve. The kurtosis value is negative for Ni and Sn.
3) The skewness coefficient of all the analyzed substances, except for the element Sn, is positive, so the spread of distributions is located to the right of the mean.

Table 1 also gives the anomalous threshold, the enrichment or depletion coefficient and the distribution of these elements. The elements Co, Mn, Ni and Zn are characterized by a normal distribution.

Table 1. *Statistics of elements.*

Elts	**Ag**	**As**	**Co**	**Cr**	**Cu**	**Fe**	**Mn**	**Mo**	**Ni**	**Pb**	**Sb**	**Sn**	**U**	**Zn**
Statistics	**(ppm)**	**(ppm)**	**(ppm)**	**(ppm)**	**(ppm)**	**(%)**	**(ppm)**	**(ppm)**	**(ppm)**	**(ppm)**	**(ppm)**	**(ppm)**	**(ppm)**	**(ppm)**
Nb. Sample	209	209	209	209	209	209	209	209	209	209	209	209	209	209
Min	0.00	0.00	7.50	20.00	1.30	0.30	50.00	0.00	65.00	0.00	0.00	0.00	0.50	20.00
Mean	1.52	1.20	27.57	94.30	6.42	2.23	236.00	1.84	331.82	18.77	1.54	1.51	1.80	74.22
Standard err.	0.12	0.09	0.89	4.68	0.29	0.08	7.03	0.14	10.94	1.03	0.17	0.06	0.08	2.55
Median	0.2	0.9	25	78.75	5	1.9	225	1.3	325	15.5	1.5	2	1.6	65
Mode	0	0	17.5	75	5	1.3	250	1.3	250	2.5	0	2	1.1	42.5
Variance	3.26	1.88	166.70	4508.80	17.41	1.26	10330.24	4.39	25009.55	222.09	6.32	0.77	1.44	1357.73
Kurtosis	0.70	6.87	0.50	28.14	1.68	0.31	0.09	28.63	-0.86	2.52	14.38	-0.38	24.09	3.08
Asym. coef	0.97	2.15	0.91	3.84	1.32	0.90	0.64	4.17	0.21	1.39	3.31	-1.06	3.56	1.58
Plage	8	9	67.5	662.5	21.2	6	500	20	682	85	18	4	11.8	215
Std dev	1.81	1.37	12.98	67.15	4.20	1.13	100.40	2.11	158.32	14.95	2.53	0.88	1.19	37.03
Mean.+ 2 σ	5.14	3.94	53.53	228.60	14.82	4.49	436.81	6.06	648.47	48.66	6.61	3.28	4.18	148.28
Max	8.00	9.00	75.00	682.50	22.50	6.30	550.00	20.00	747.00	85.00	18.00	4.00	11.80	235.00
Clarke	0.08	1.80	25.00	102.00	60.00	56300	1050.00	1.20	84.00	14.00	0.20	2.30	2.70	70.00
Mean - 2 σ	-2.10	-1.54	1.60	-39.99	-1.98	-0.03	35.20	-2.38	15.17	-11.13	-3.52	-0.25	-0.57	0.17
distrib. law	Log. norm	Log. norm	Normale	Log. norm	Log. norm	Log. norm	Normale	Log. norm	Normale	Log. norm	Log. norm	Log. norm	Log. norm	Normale
Mean/Clarke	20.26	0.67	1.10	0.92	0.11	0.00	0.22	1.53	3.95	1.34	7.71	0.66	0.67	1.06

The means of all the chemical elements, except Sn, are higher than their median values, which also reflect that the distribution of the grade has right deviation.

The monovariate statistic gives the geochemical anomaly threshold of the analyzed chemicals. This geochemical threshold can also be determined using the cumulative frequency curve (Table 2), as shown in the graphs of Figure 3 (Cf. Ag graph).

Table 2. *Normal thresholds of the elements.*

Substances	Ag	As	Co	Cr	Cu	Fe	Mn	Mo	Ni	Pb	Sb	Sn	U	Zn
Statistics	**(ppm)**	**(ppm)**	**(ppm)**	**(ppm)**	**(ppm)**	**(ppm)**	**(ppm)**	**(ppm)**	**(ppm)**	**(ppm)**	**(ppm)**	**(ppm)**	**(ppm)**	**(ppm)**
Abnormal thereshold	5,10	6,60	65,00	260,00	15,00	5,00	500,00	7,50	680,00	62,50	12,00	2,00	5,90	200,00
Moy.+2 Std	5,14	3,94	53,53	228,60	14,82	4,49	436,81	6,06	648,47	48,66	6,61	3,28	4,18	148,28

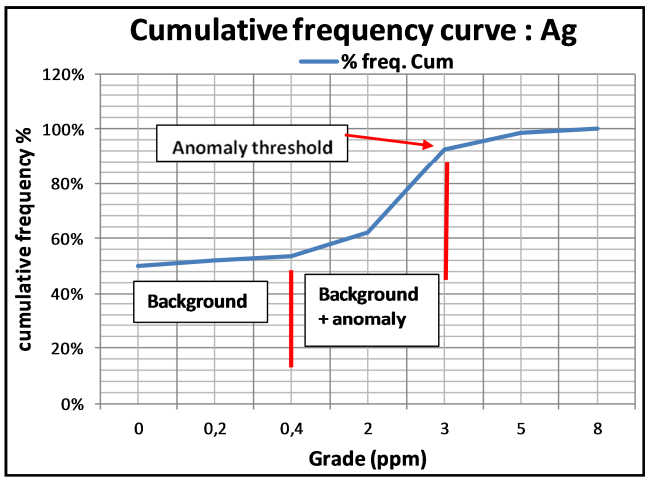

Figure 3. *Determination of the anomaly threshold using the cumulative frequency curve (Cf. Ag graph).*

On the cumulative frequency curve of Ag, the anomalous threshold is at 5.1 ppm. This threshold was determined by the monovariate statistical method, of the mean plus two (2) times the standard deviation (Mean +2σ) is 5.14 ppm (Table 2).

4.1.2. Multivariate Statistical Analysis

The multivariate analysis [30] gives the Pearson correlation matrix (Table 3) which reveals that the substances with the highest coefficients are:

Ni-Cr (0.644), Cu-Co (0.619), Fe-Co (0.601), Sb-Mo (0.588), Fe-Cu (0.536), Zn-Co (0.530), Zn-Cu (0.511), Zn-Mn (0.506), Zn-Fe (0.480), Pb-Cu (0.455), Pb-Co (0.428), Mn-Fe (0.441) Mn-Cu (0.401).

The factorial analysis highlighted the relationships existing between the mineral substances and their classification according to their concordance with the factorial axis (Tables 4 and 5).

The first two factors F1 and F2 concentrate the greatest percentages of variability (Table 4), which is reflected in the histogram in Figure 4.

The result of this factor analysis allows data structure understanding [8-10, 14, 16, 19, 26], delineating the geochemical domains and interpreting the geological domains (see Table 5) [29].

Table 3. *Pearson correlation matrix.*

Variables	Ag	As	Co	Cr	Cu	Fe	Mn	Mo	Ni	Pb	Sb	Sn	U	Zn
Ag	1	-0,034	0,008	0,078	0,032	0,026	0,051	-0,193	0,056	0,169	-0,115	0,113	-0,057	-0,126
As	-0,034	1	0,154	0,049	0,054	0,112	0,032	-0,033	0,075	0,126	-0,046	-0,041	-0,007	-0,006
Co	0,008	0,154	1	-0,174	0,619	0,601	0,346	0,129	-0,381	0,428	0,036	0,048	0,261	0,530
Cr	0,078	0,049	-0,174	1	-0,107	-0,057	0,025	-0,224	0,644	0,043	-0,168	-0,100	-0,086	-0,050
Cu	0,032	0,054	0,619	-0,107	1	0,536	0,401	0,188	-0,312	0,455	0,057	-0,039	0,156	0,511
Fe	0,026	0,112	0,601	-0,057	0,536	1	0,441	-0,054	-0,184	0,378	-0,078	0,054	0,133	0,480
Mn	0,051	0,032	0,346	0,025	0,401	0,441	1	-0,069	0,080	0,248	0,002	0,015	0,018	0,506
Mo	-0,193	-0,033	0,129	-0,224	0,188	-0,054	-0,069	1	-0,245	0,071	0,588	0,070	0,299	-0,035
Ni	0,056	0,075	-0,381	0,644	-0,312	-0,184	0,080	-0,245	1	-0,352	-0,224	-0,075	-0,135	-0,192
Pb	0,169	0,126	0,428	0,043	0,455	0,378	0,248	0,071	-0,352	1	0,066	0,142	0,094	0,225
Sb	-0,115	-0,046	0,036	-0,168	0,057	-0,078	0,002	0,588	-0,224	0,066	1	0,127	0,292	-0,036
Sn	0,113	-0,041	0,048	-0,100	-0,039	0,054	0,015	0,070	-0,075	0,142	0,127	1	0,039	-0,009
U	-0,057	-0,007	0,261	-0,086	0,156	0,133	0,018	0,299	-0,135	0,094	0,292	0,039	1	0,050
Zn	-0,126	-0,006	0,530	-0,050	0,511	0,480	0,506	-0,035	-0,192	0,225	-0,036	-0,009	0,050	1

Table 4. *Eigen values.*

	F1	F2	F3	F4	F5	F6	F7	F8	F9
Eigen Values	3,176	1,802	0,948	0,617	0,356	0,216	0,112	0,096	0,031
Variability (%)	22,686	12,871	6,769	4,410	2,546	1,541	0,798	0,687	0,220
Cumulative (%)	22,686	35,557	42,326	46,736	49,282	50,823	51,621	52,309	52,529

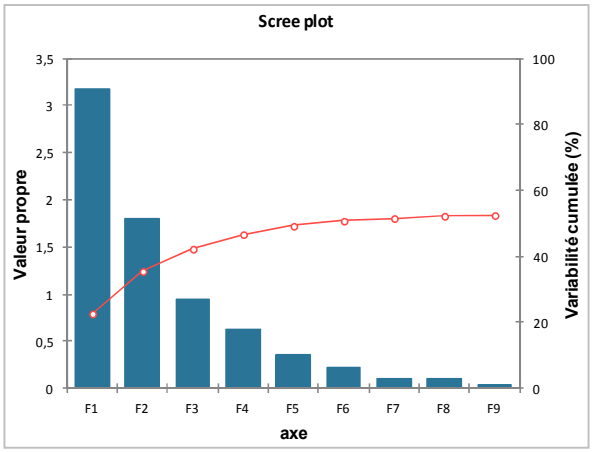

Figure 4. Scree plot.

The factorial coordinates obtained (Table 5) are represented graphically as a function of the factors F1 and F2, on the x-axis and y-axis respectively. The Figure 5 shows that the substances Cu, Co and Pb have a strong correlation as well as Fe and Zn on the one hand, and Sb and Mo on the other. The grades of Ni and Cr on the one hand, and Sn, U, Sb, Mo on the other hand, vary inversely.

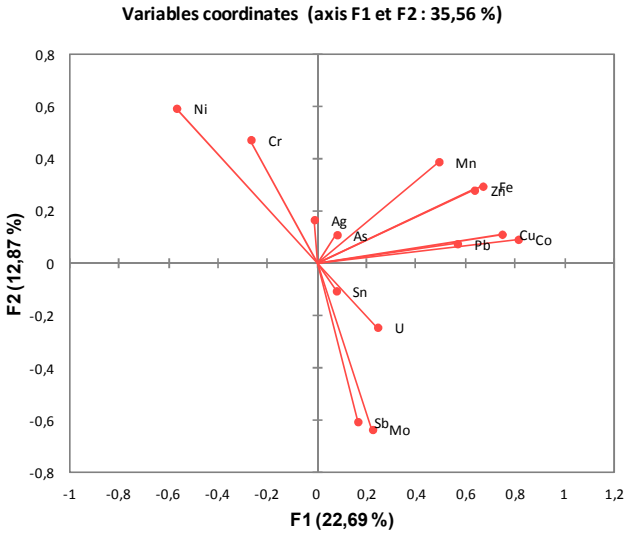

Figure 5. Representation of the minerals in the factorial coordinates.

Table 5. Factor coordinates.

	F1	F2	F3	F4	F5	Initiale Communality	finale Communality	spécific Variance
Ag	-0,012	0,168	-0,118	0,353	-0,174	0,137	0,197	0,803
As	0,080	0,110	0,040	0,095	0,196	0,089	0,068	0,932
Co	0,812	0,093	0,005	0,009	0,233	0,590	0,722	0,278
Cr	-0,268	0,473	0,338	0,218	0,101	0,537	0,467	0,533
Cu	0,746	0,112	0,081	0,018	0,070	0,537	0,582	0,418
Fe	0,669	0,296	0,008	-0,003	0,051	0,478	0,537	0,463
Mn	0,491	0,390	0,217	-0,146	-0,341	0,422	0,578	0,422
Mo	0,224	-0,634	0,426	-0,001	0,070	0,443	0,638	0,362
Ni	-0,568	0,593	0,568	-0,002	0,043	0,653	1,000	0,000
Pb	0,566	0,076	-0,037	0,512	-0,041	0,454	0,591	0,409
Sb	0,164	-0,604	0,445	0,055	-0,173	0,401	0,622	0,378
Sn	0,077	-0,104	-0,002	0,181	-0,193	0,085	0,087	0,913
U	0,244	-0,243	0,231	0,039	0,127	0,177	0,190	0,810
Zn	0,635	0,281	0,052	-0,339	-0,085	0,487	0,606	0,394

Applying the rotation by choosing the two first factors F1 and F2 (Cf. Figure 6), to summarize the features, reduces the factorial coordinates to two (2), D1 and D2 (Table 6) which graphical representation is shown by Figure 7. The first two of the five factors account for 35.56% of the common variability of all fourteen substances analyzed (Figure 6).

The factorial analysis of termite geochemistry results reveals five main groups, namely:

1) Cu-Co-Pb;
2) Fe-Zn, Mn-As;
3) Sb-Mo;
4) Sn-U;
5) Ni-Cr.

Substances: (Cu, Co, Pb), (Zn, Fe), (Mn, As) are positively correlated. The elements (U, Sn) are positively correlated, as well as (Sb, Mo). Both groups have a positive correlation. When U grade increases, Sn grade increases as well as Sb and Mo.

The minerals (Sb, Mo) and (Zn, Fe) as well as (Sn, U) and Mn are independent.

The group (Ni, Cr, Ag) has a negative correlation with the group (Mo, Sb, U, Sn); this means that when the grade of Ni, Cr or Ag increases the grade of Mo, Sb, U and Sn decreases.

Sn, As and Ag are not well represented by the selected F1 and F2 factors.

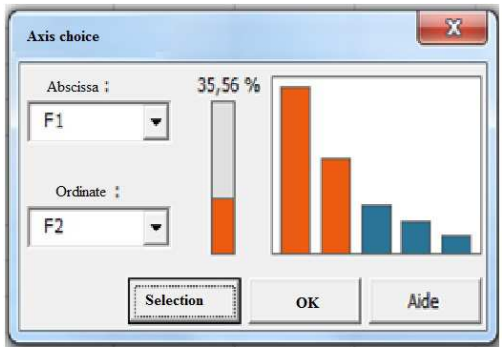

Figure 6. Result of the axis choice.

Table 6. *Factor coordinates.*

	D1	D2
Ag	0,059	-0,158
As	0,118	-0,068
Co	0,778	0,250
Cr	-0,049	-0,542
Cu	0,726	0,205
Fe	0,731	0,006
Mn	0,608	-0,152
Mo	-0,058	0,669
Ni	-0,273	-0,775
Pb	0,547	0,164
Sb	-0,100	0,617
Sn	0,027	0,127
U	0,122	0,322
Zn	0,694	0,006

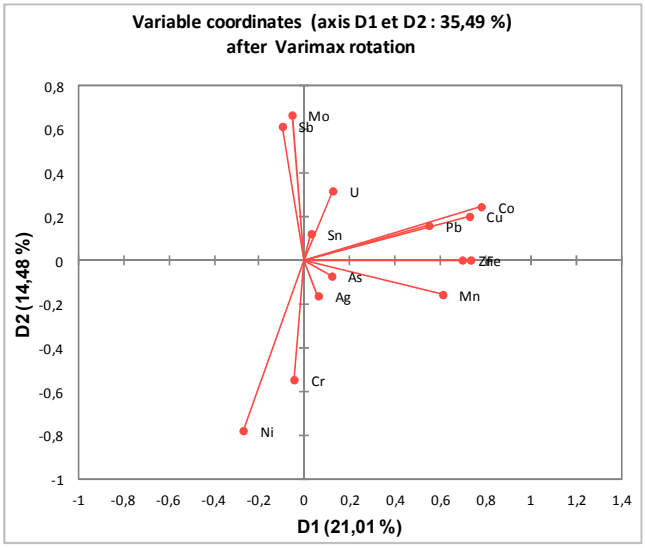

Figure 7. *Graph of the variables.*

Table 7. *Correlations between variables and factors after Varimax rotation.*

	D1	D2
Ag	0,062	-0,165
As	0,126	-0,071
Co	0,829	0,261
Cr	-0,052	-0,566
Cu	0,774	0,215
Fe	0,779	0,007
Mn	0,648	-0,159
Mo	-0,061	0,700
Ni	-0,291	-0,810
Pb	0,583	0,171
Sb	-0,106	0,645
Sn	0,029	0,132
U	0,130	0,337
Zn	0,740	0,006

The correlation table between the variables and the factors generated after the application of the Varimax rotation function (Table 7) represented graphically (Figure 8) confirms the previous conclusions.

The graph of observations (Figure 9) highlights the relationships between the geochemical elements on the one hand, and the elements and observations on the other.

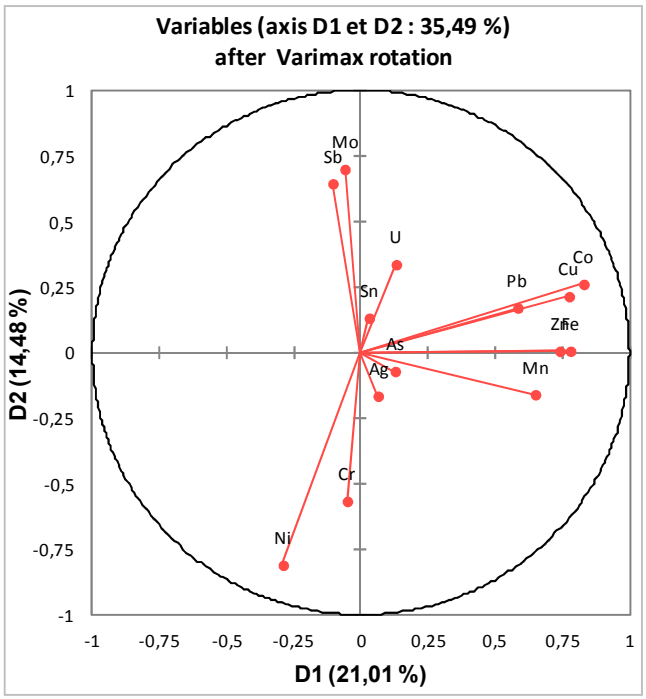

Figure 8. *Representation of the variables as a function of the factors after rotation.*

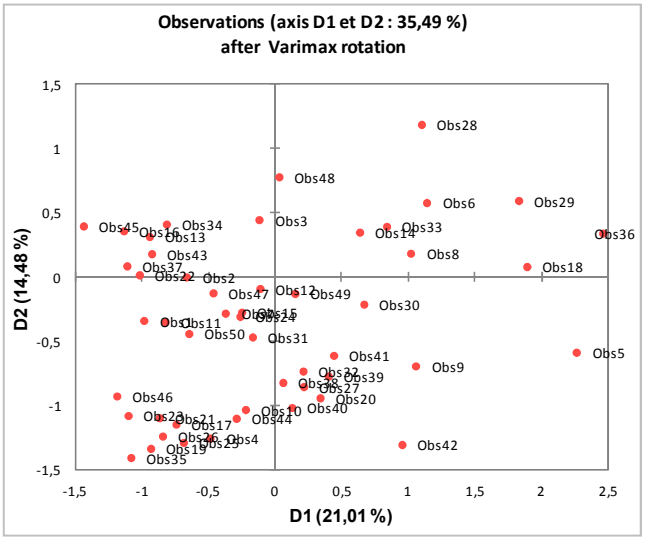

Figure 9. *Representation of the observations in the graph after the Varimax rotation.*

The table 8 shows the correspondence between the observations (D1>0, D2>0) and the termite mound samples. The elements Co, Cu, Fe, Pb, Sn, U and Zn show high and comparable levels in these samples along the D1 and D2 axis.

Table 8. *Relationship between observations and termite mound samples.*

Observation	F1	F2	F3	F4	F5	Sample	Co	Cu	Fe	Pb	Sn	U	Zn
Obs6	1,279	-0,064	-1,620	-0,274	1,126	7	50	7,5	4	25	0	2	82,5
Obs8	1,006	0,246	-0,613	1,214	1,177	9	48	13	4	30	2	7	62,5
Obs14	0,724	-0,062	-1,009	1,086	1,000	28	45	5	3	43	2	2	60
Obs18	1,761	0,701	-0,133	-1,224	-0,933	32	33	15	4	28	2	2	188
Obs28	1,495	-0,635	0,486	1,114	0,838	51	45	15	4	38	2	4	65
Obs29	1,916	0,207	0,572	1,480	1,433	52	55	18	5	50	2	4	75
Obs33	0,928	-0,019	-0,551	0,593	0,519	56	38	10	4	35	2	2	57,5
Obs36	2,389	0,700	-0,570	-0,167	0,325	59	60	23	5	15	2	1	135
Obs48	0,349	-0,705	-1,217	-0,049	0,970	80	35	7,5	1	20	0	2	77,5

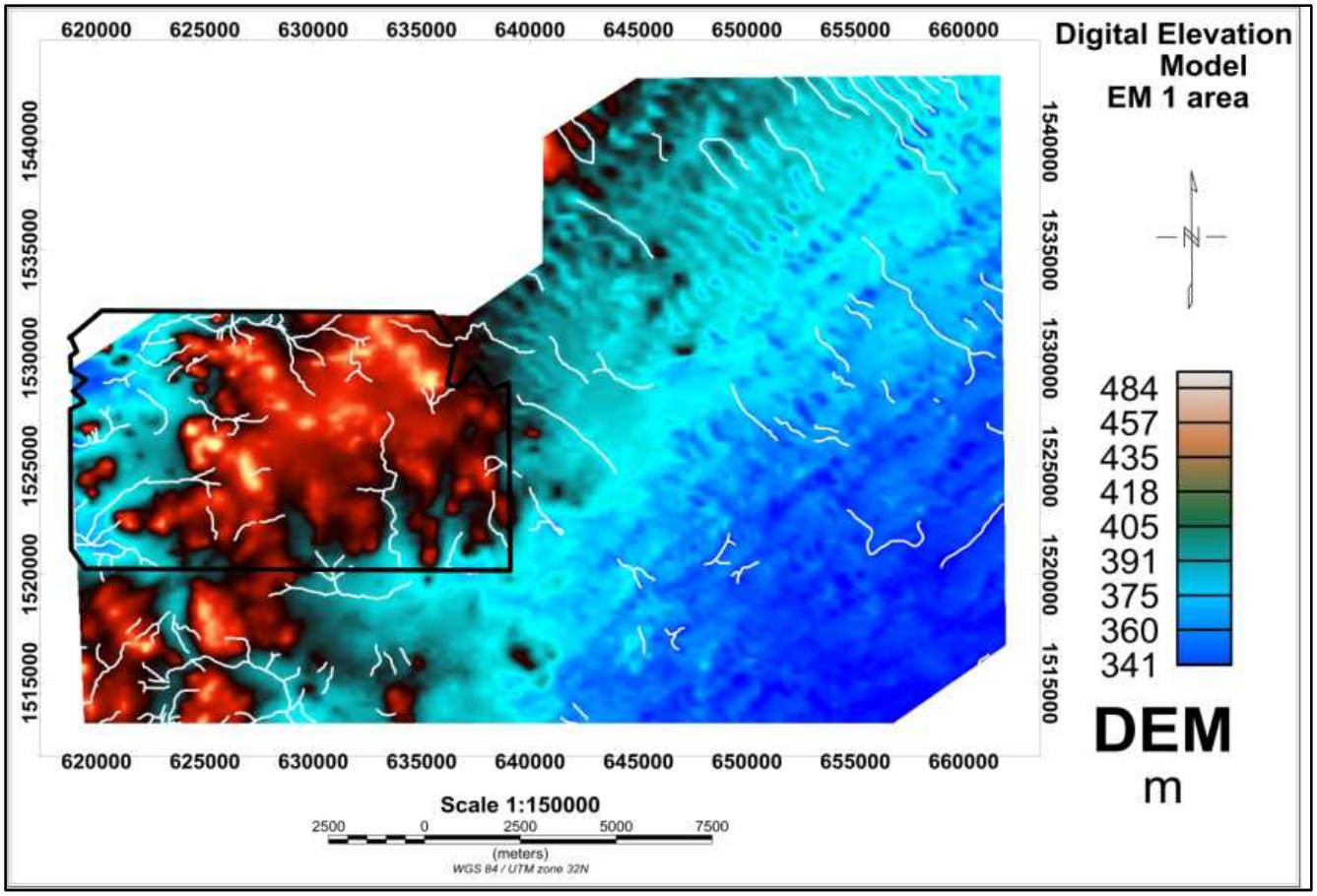

Figure 10. *Digital Elevation Model (DEM) of target EM_1.*

4.2. Digital Terrain Model and Hydrographic Network

The EM_1 area covered by the termite mound geochemistry is characterized by a very uneven topography in the central and eastern parts. Indeed, the altitude of the area varies from 341.26 m to 520.07 m, i.e. a difference in altitude of 178.81 m (Figure 10). The lowest elevation is in the southeast of the area covered by the termite mound geochemistry (DEM map). The hydrographic network, shown in white color, in the geochemical survey area is secondary. These are essentially koris that originate from the mountain slopes.

4.3. Geophysical Interpretations

The geophysical data were processed and used to produce maps (Figure 11) including the Total Magnetic Field, the horizontal and vertical derivatives, the analytical signal, and the resistivity map for the 56000 Hz frequency. Geophysical data and satellite images were used for structural interpretation.

The magnetic maps, notably the total magnetic field (A), the derivatives (B and C) show units with high magnetic intensity in the western and eastern half of the map (Figure 11-A, B and C). The analytical signal map (D) shows that these are well circumscribed units. The resistivity map (E) shows that these magnetic units are characterized by conductive zones, especially in the Northwest, the Southwest and the Southeast.

The total magnetic field and vertical and horizontal derivative maps show long-linear magnetic anomalies and lineaments oriented N45° to N70° and N120° to 160° (F).

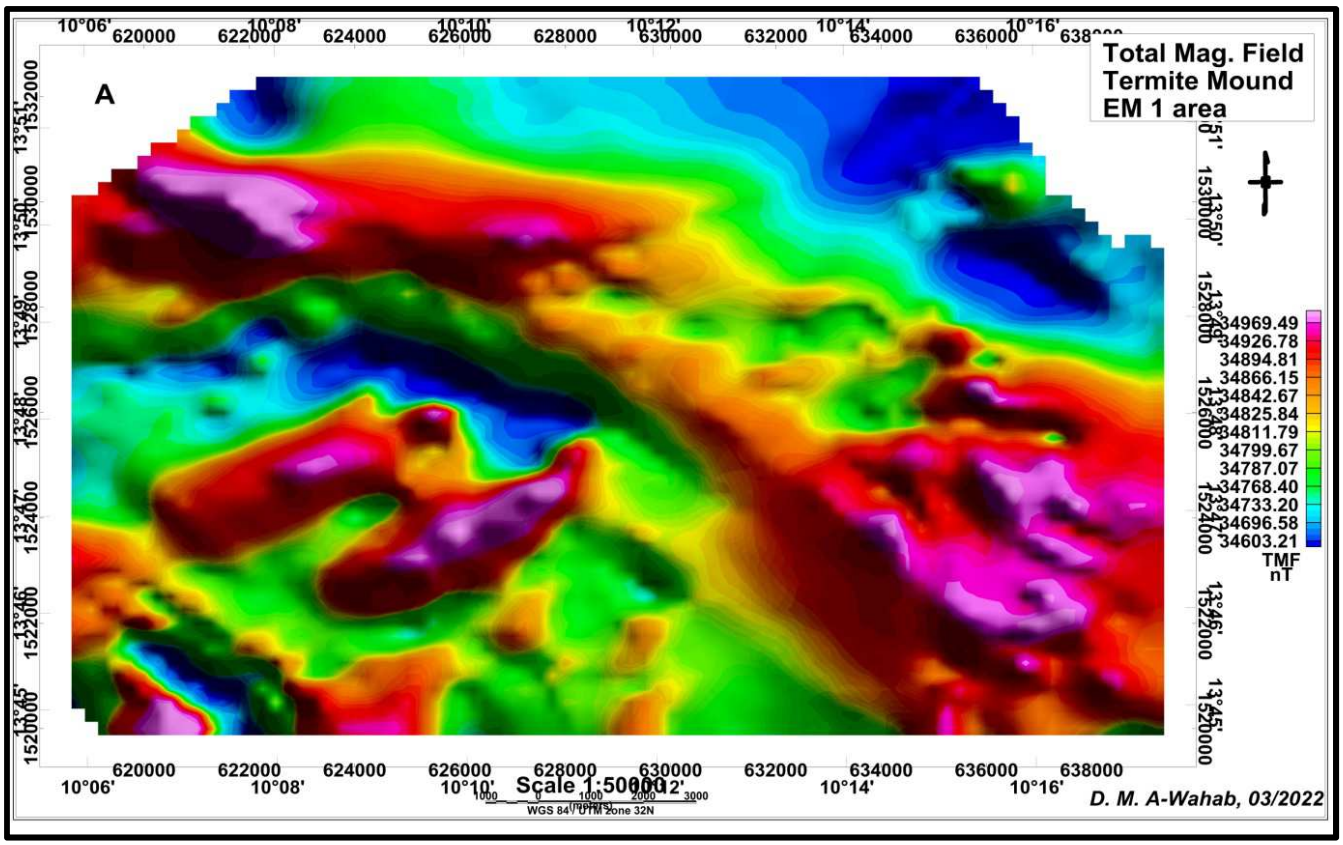
A
Total Mag. Field
Termite Mound
EM 1 area
34969.49
34926.78
34894.81
34866.15
34842.67
34825.84
34811.79
34799.67
34787.07
34768.40
34733.20
34696.58
34603.21
TMF
nT
Scale 1:50000
WGS 84 / UTM zone 32N
D. M. A-Wahab, 03/2022

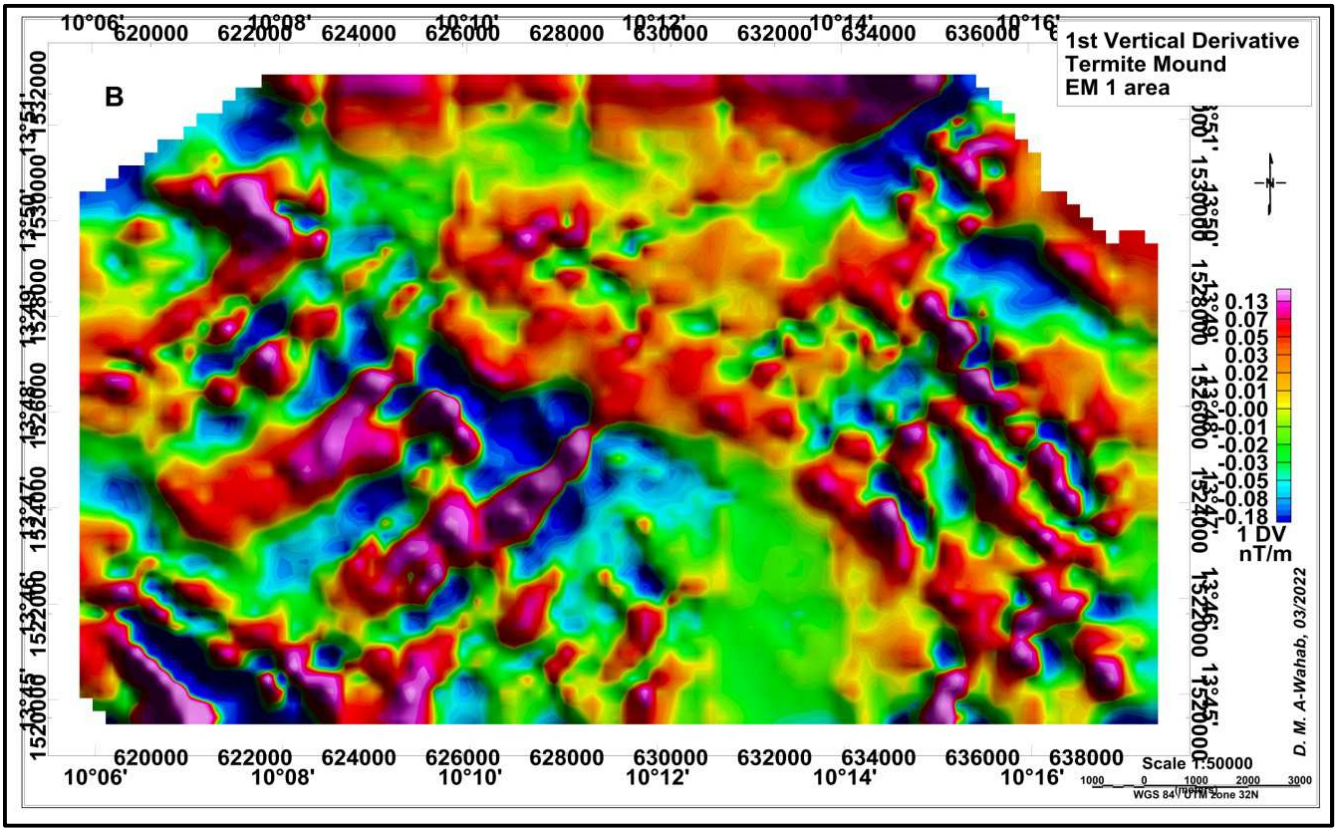
B
1st Vertical Derivative
Termite Mound
EM 1 area
0.13
0.07
0.05
0.03
0.02
0.01
-0.00
-0.01
-0.02
-0.03
-0.05
-0.08
-0.18
1 DV
nT/m
Scale 1:50000
WGS 84 / UTM zone 32N
D. M. A-Wahab, 03/2022

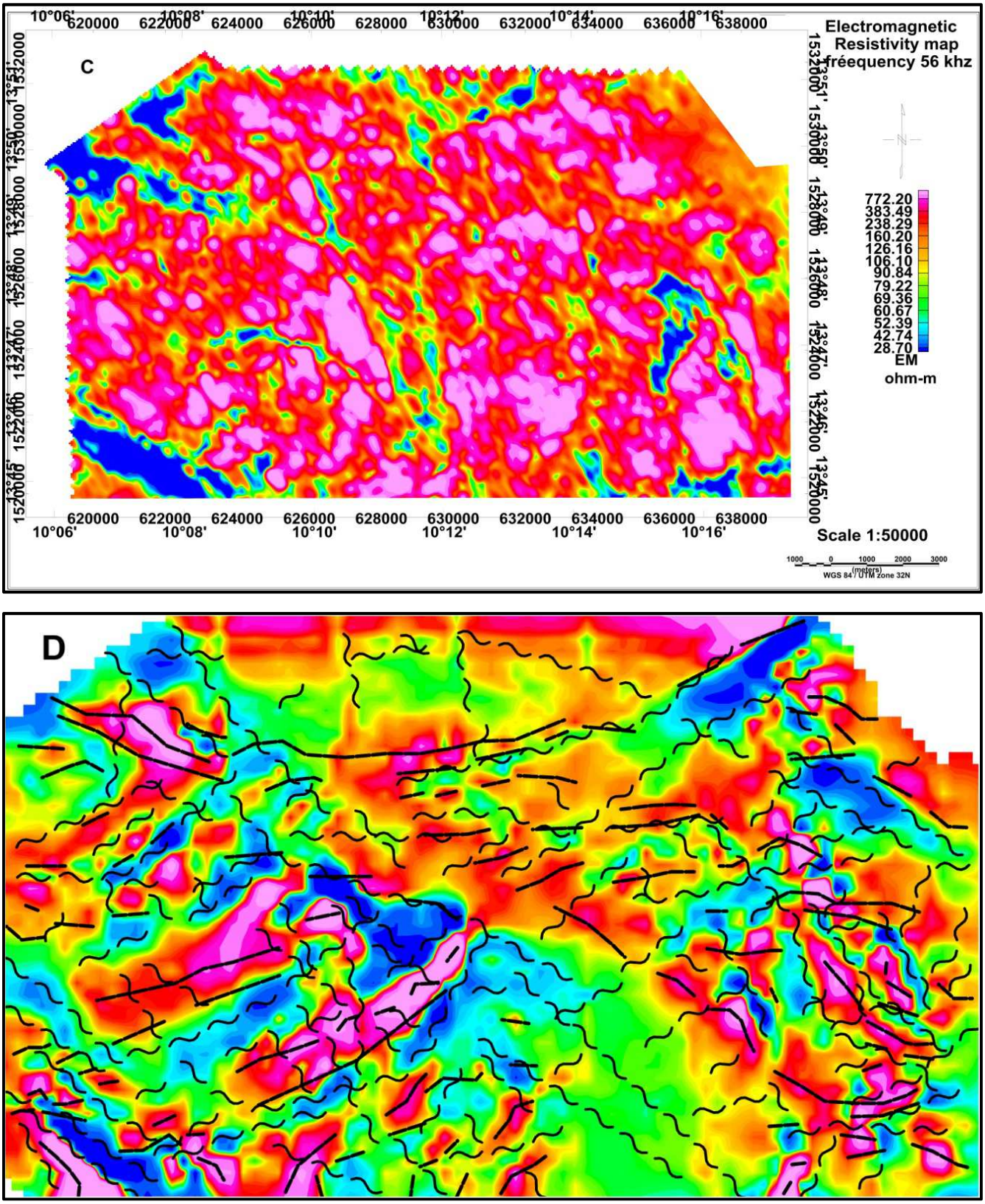

Figure 11. *Geophysical maps: Total magnetic field (TMI) (A), Map of the 1st vertical derivative (B), Shaded map of the Horizontal gradient (C), Analytical signal map (D), Resistivity map, freq 56000 Hz (E), Interpretation map of the faults and geophysical lineaments on the 1DV (F).*

4.4. Structural Interpretation of Satellite Imagery

Landsat 8 imageries were used to perform image analysis by bands combinations: 7, 4, 1 (A), 6, 5, 3 (B) and the ratio 7/5, 7/4, 5/1 (C) etc... The satellite imageries were used for structural analysis and interpretation [32]. Before doing this,

the satellite imageries were processed by using several methods, notably SOBEL filters (Table 9) to highlight structures in different directions. The images (A) and (B) result from the application of the NE-SW and NW-SE filters (Figure 12). The NE-SW filter highlighted the NW-SE and N-S structures while the NW-SE filter highlighted the NE-SW and E-W structures.

Table 9. *Matrices of the applied SOBEL filters.*

1	1	1	2	1	1	1	-1	-1	-1	0	1	1	1
1	1	2	3	2	2	1	-1	-1	-2	0	2	1	1
1	2	3	4	3	3	1	-1	-2	-3	0	3	2	1
0	0	0	0	0	0	0	-2	-3	-4	0	4	3	2
-1	-2	-3	-4	-3	-3	-1	-1	-2	-3	0	3	2	1
-1	-1	-2	-3	-2	-2	-1	-1	-1	-2	0	2	1	1
-1	-1	-1	-2	-1	-1	-1	-1	-1	-1	0	1	1	1
		SOBEL NS							SOBEL EW				

0	1	1	1	1	1	2	2	1	1	1	1	1	0
-1	0	2	2	2	3	1	1	3	2	2	2	0	1
-1	-2	0	3	4	2	1	1	2	4	3	0	-2	-1
-1	-2	-3	0	3	2	1	1	2	3	0	-3	-2	-1
-1	-2	-4	-3	0	2	1	1	2	0	-3	-4	-2	-1
-1	-3	-2	-2	-2	0	1	1	0	-2	-2	-2	-3	-1
-2	-1	-1	-1	-1	-1	0	0	-1	-1	-1	-1	-1	-2
		SOBEL NE-SW							SOBEL NW-SE				

The structures and lineaments observed on the satellite images have almost the same orientation (Figure 12-D) as those interpreted by geophysics.

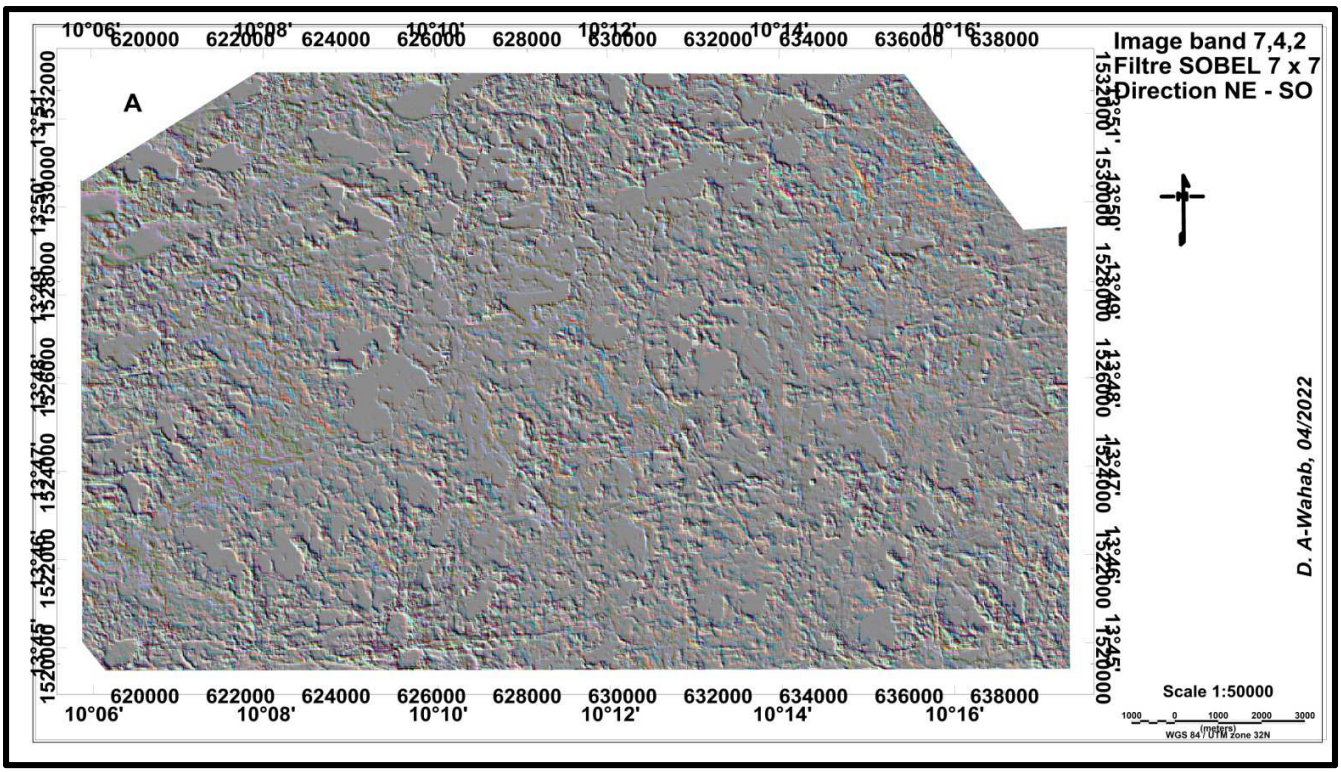

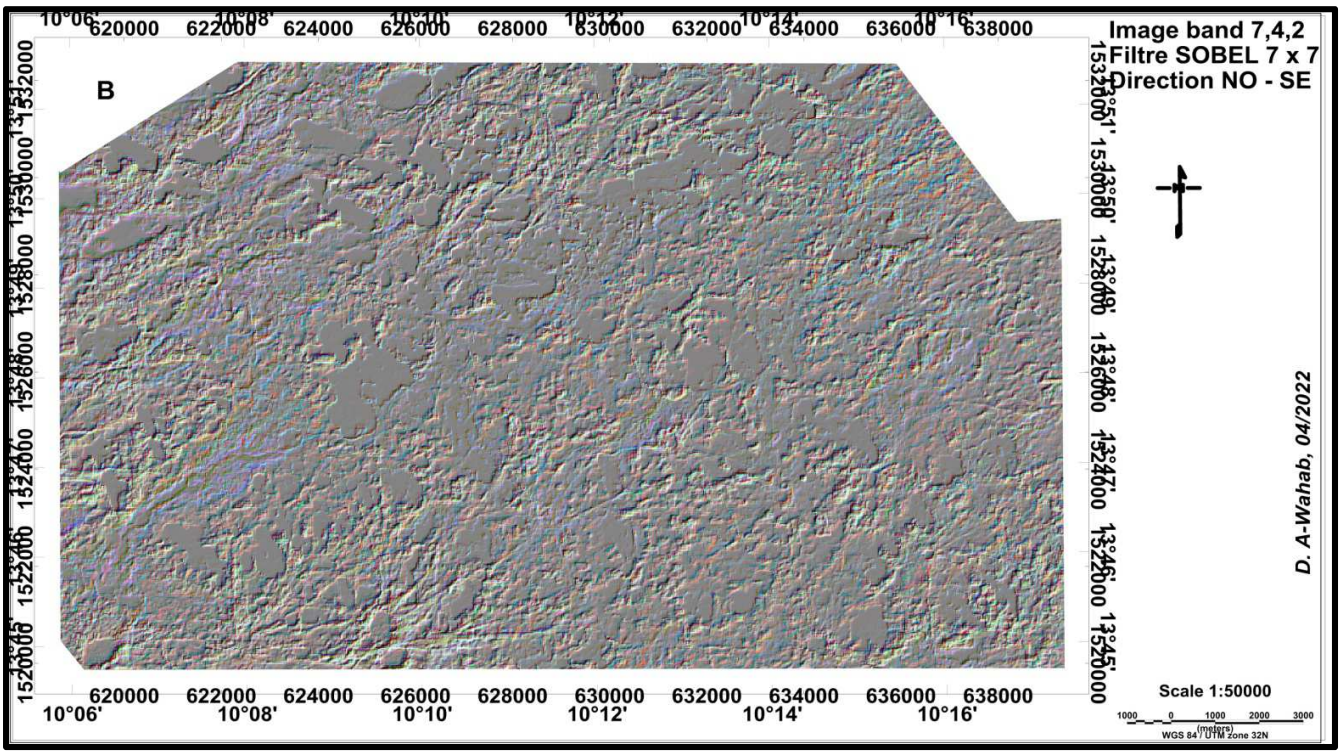
B
Image band 7,4,2
Filtre SOBEL 7 x 7
Direction NO - SE
D. A-Wahab, 04/2022
Scale 1:50000
1000 0 1000 2000 3000
(meters)
WGS 84 / UTM zone 32N
10°06' 10°08' 10°10' 10°12' 10°14' 10°16'
620000 622000 624000 626000 628000 630000 632000 634000 636000 638000

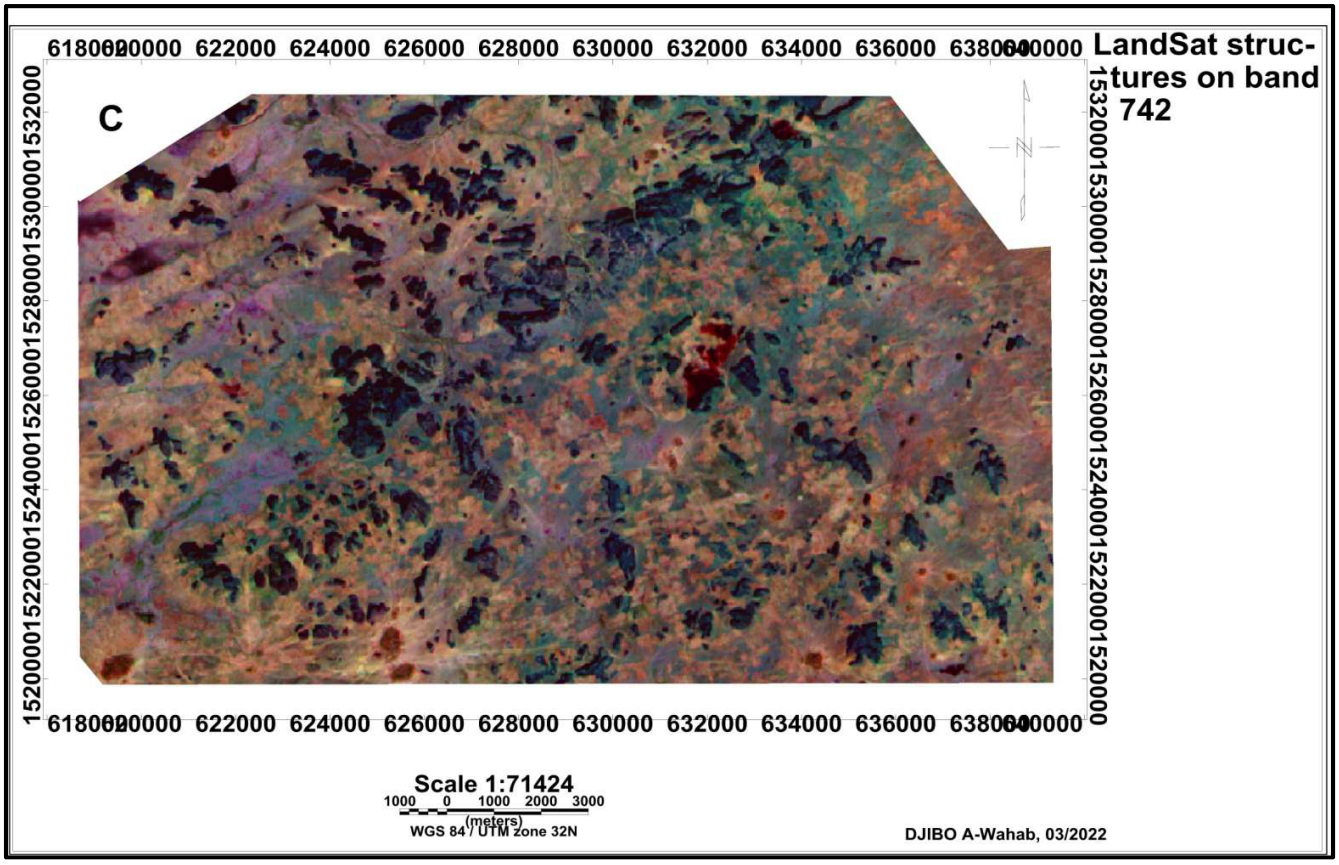
C
LandSat structures on band 742
Scale 1:71424
1000 0 1000 2000 3000
(meters)
WGS 84 / UTM zone 32N
DJIBO A-Wahab, 03/2022
618000 620000 622000 624000 626000 628000 630000 632000 634000 636000 638000 640000
1532000 1530000 1528000 1526000 1524000 1522000 1520000

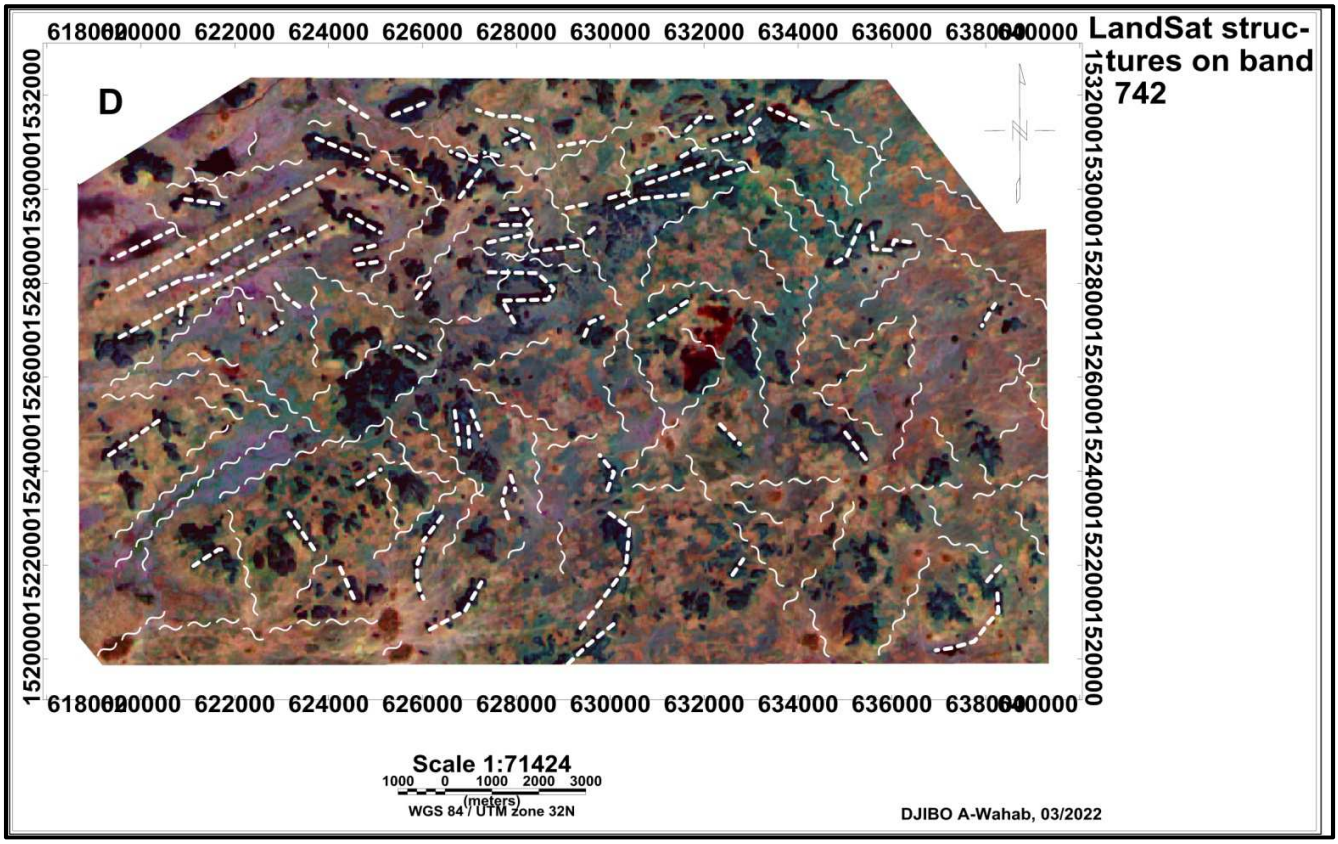

Figure 12. *LandSat 8 imagery: SOBEL 7x7 NE-SW filter application (A), SOBEL 7x7 NW-SE filter application (B) 7,4,1 band combination (C), Interpretation map of LandSat faults and lineaments on image 7,4,1 (D).*

The map (Figure 13) is a synthesis of geophysical data and structural interpretations of satellite imageries.

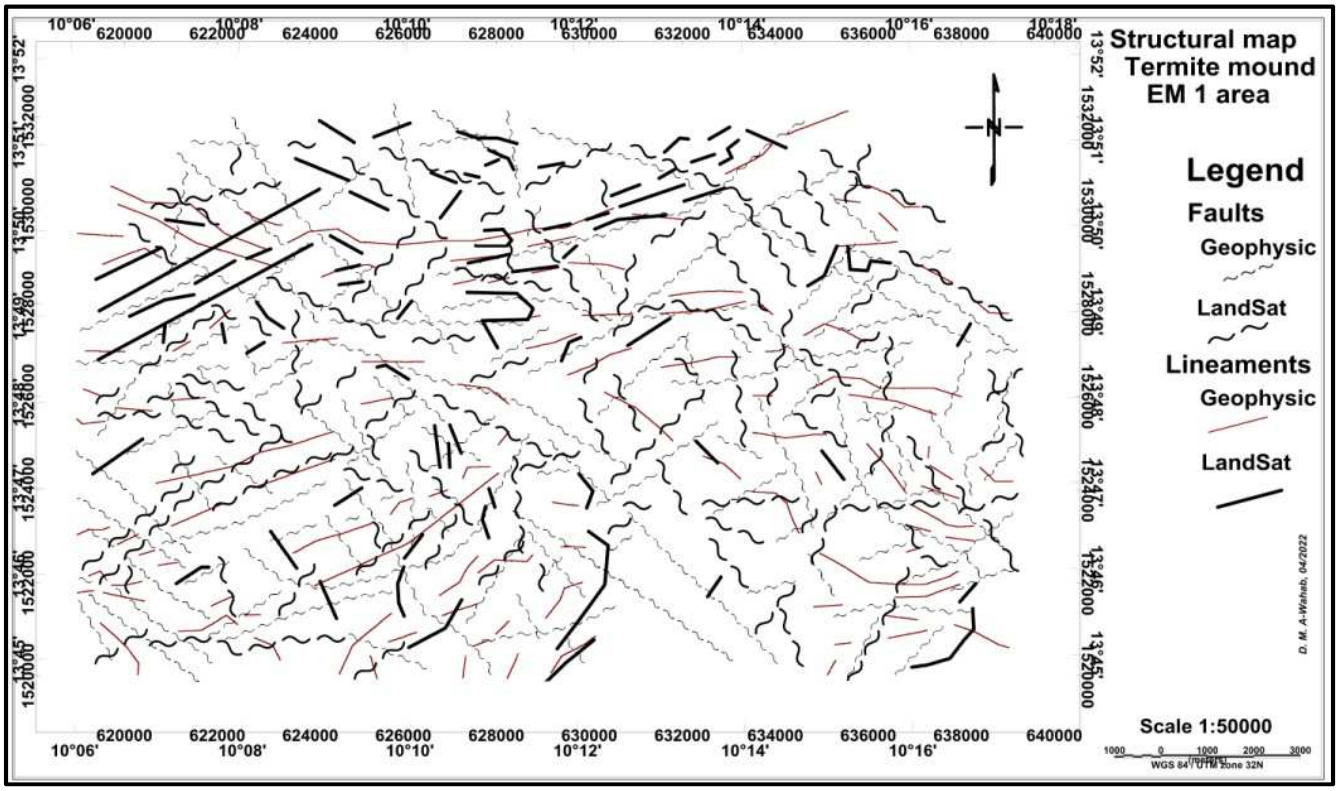

Figure 13. *Structural synthesis map.*

All the structural elements have been analyzed and the results are presented in Figure 14.

The interpretation of the geophysical faults reveals two main directions of the structures, namely N50° to N70° and N130° to N140° (Figure 14-A). The magnetic lineaments are oriented N60° to N100° (Figure 14-B).

The Landsat faults are oriented N45° to N60°, N120° to 130° and N140° to N170 ° (Figure 14-C). Landsat lineaments are oriented N60° to N70°(Figure 14-D).

The direction average of faults interpreted by geophysical data is N98.6° and that of faults interpreted by satellite imagery is N96.3°.

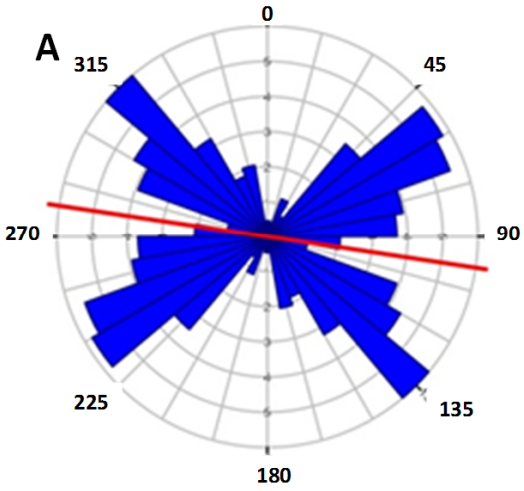

Rose Diagram	
Statistical Summary	
Calculation Method	Frequency
Class interval	10.0 Degrees
Data type	Bidirectional
Population	217
Total Length of All Lineations	4.8
Maximum Bin Population	26.0
Mean Bin Population	12.06
Standard Deviation of Bin Population	8.18
Maximum Bin Population (%)	5.99
Mean Bin Population (%)	2.78
Standard Deviation of Bin Population (%)	1.88
Maximum Bin Length	0.29
Mean Bin Length	0.13
Standard Deviation of Bin Lengths	0.09
Maximum Bin Lenght (%)	6.06
Mean Bin Length (%)	2.78
Standard Deviation of Bin Lengths (%)	1.69
Vector Mean	96.6 Degrees
	278.67 Degrees
Confidence Interval	12.4 Degrees
	(80 Percent)
R-mag	0.28

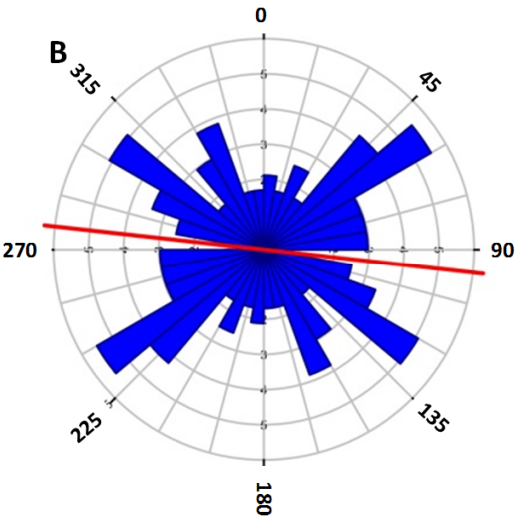

Rose Diagram	
Statistical Summary	
Calculation Method	Frequency
Class interval	10.0 Degrees
Data type	Bidirectional
Population	118
Total Length of All Lineations	3.1
Maximum Bin Population	13.0
Mean Bin Population	6.56
Standard Deviation of Bin Population	3.01
Maximum Bin Population (%)	5.51
Mean Bin Population (%)	2.78
Standard Deviation of Bin Population (%)	1.27
Maximum Bin Length	0.17
Mean Bin Length	0.09
Standard Deviation of Bin Lengths	0.04
Maximum Bin Lenght (%)	5.61
Mean Bin Length (%)	2.78
Standard Deviation of Bin Lengths (%)	1.42
Vector Mean	96.3 Degrees
	276.34 Degrees
Confidence Interval	42.8 Degrees
	(80 Percent)
R-mag	0.11

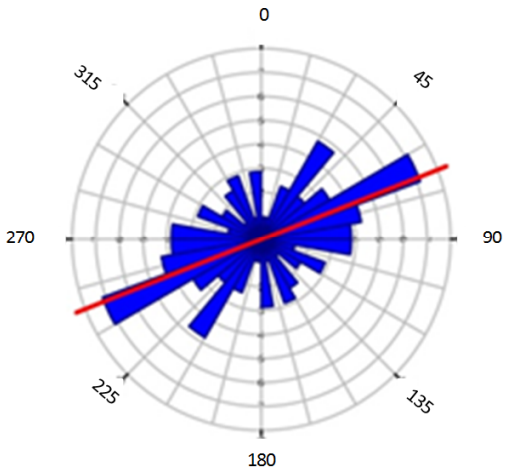

Rose Diagram	
Statistical Summary	
Calculation Method	Frequency
Class interval	10.0 Degrees
Data type	Bidirectional
Population	105
Total Length of All Lineations	147 749.15
Maximum Bin Population	15.0
Mean Bin Population	5.83
Standard Deviation of Bin Population	333
Maximum Bin Population (%)	7.14
Mean Bin Population (%)	2.78
Standard Deviation of Bin Population (%)	1.58
Maximum Bin Length	19 870.74
Mean Bin Length	4 104.14
Standard Deviation of Bin Lengths	4272.32
Maximum Bin Lenght (%)	13.45
Mean Bin Length (%)	2.78
Standard Deviation of Bin Lengths (%)	2.89
Vector Mean	68.5 Degrees
	248.67 Degrees
Confidence Interval	12.1 Degrees
	(80 Percent)
R-mag	0.4

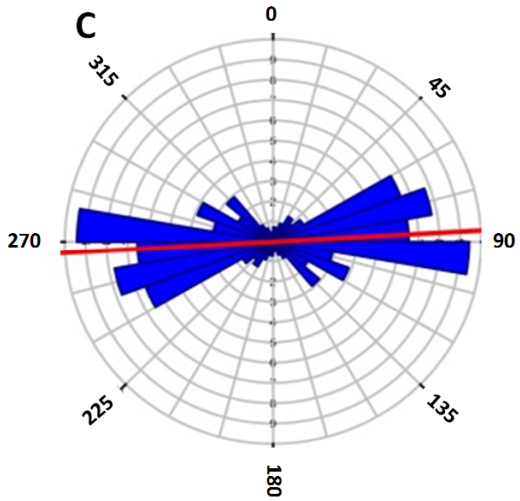

Rose Diagram	
Statistical Summary	
Calculation Method	Frequency
Class interval	10.0 Degrees
Data type	Bidirectional
Population	207
Total Length of All Lineations	2.21
Maximum Bin Population	39.0
Mean Bin Population	12.94
Standard Deviation of Bin Population	11.63
Maximum Bin Population (%)	9.42
Mean Bin Population (%)	3.13
Standard Deviation of Bin Population (%)	2.81
Maximum Bin Length	0.21
Mean Bin Length	0.07
Standard Deviation of Bin Lengths	0.07
Maximum Bin Lenght (%)	9.35
Mean Bin Length (%)	3.12
Standard Deviation of Bin Lengths (%)	3.12
Vector Mean	86.8 Degrees
	266.77 Degrees
Confidence Interval	4.6 Degrees
	(80 Percent)
R-mag	0.67

Figure 14. *Rosettes (A) Geophysical faults, (B) Geophysical lineaments, (C) Landsat faults, (D) LandSat lineaments.*

Cu-Co-Pb-Fe anomalies

The copper map shows four (4) anomalous zones a, b, c and d (Figure 15):

1) In zone (a), Cu is associated with Co, Pb and Fe, whose values are maximum;
2) Cu grade is maximum throughout the (b) zone, while Co, Pb and Fe are mostly found in the center and south;
3) Cu grade is medium to high in zone (c) while Co, Pb and Fe are found associated with Cu in the northern and southern extremities of the DMP;

4) Cu, Co, Pb and Fe are closely associated in the (d) zone. The eastern center of anomaly (b) and the west of (c) show conductive zones. Anomaly (d) is characterized by a strong potassium grade.

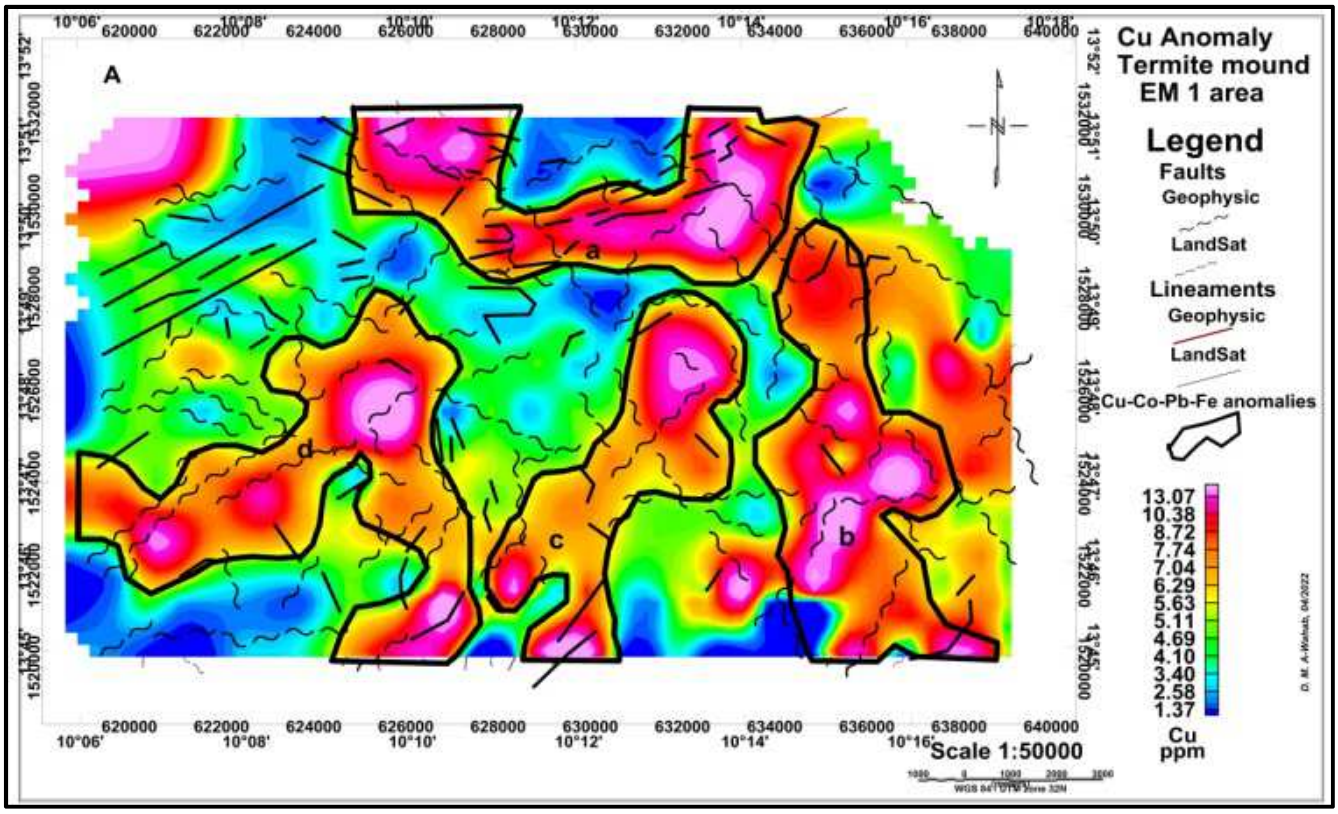

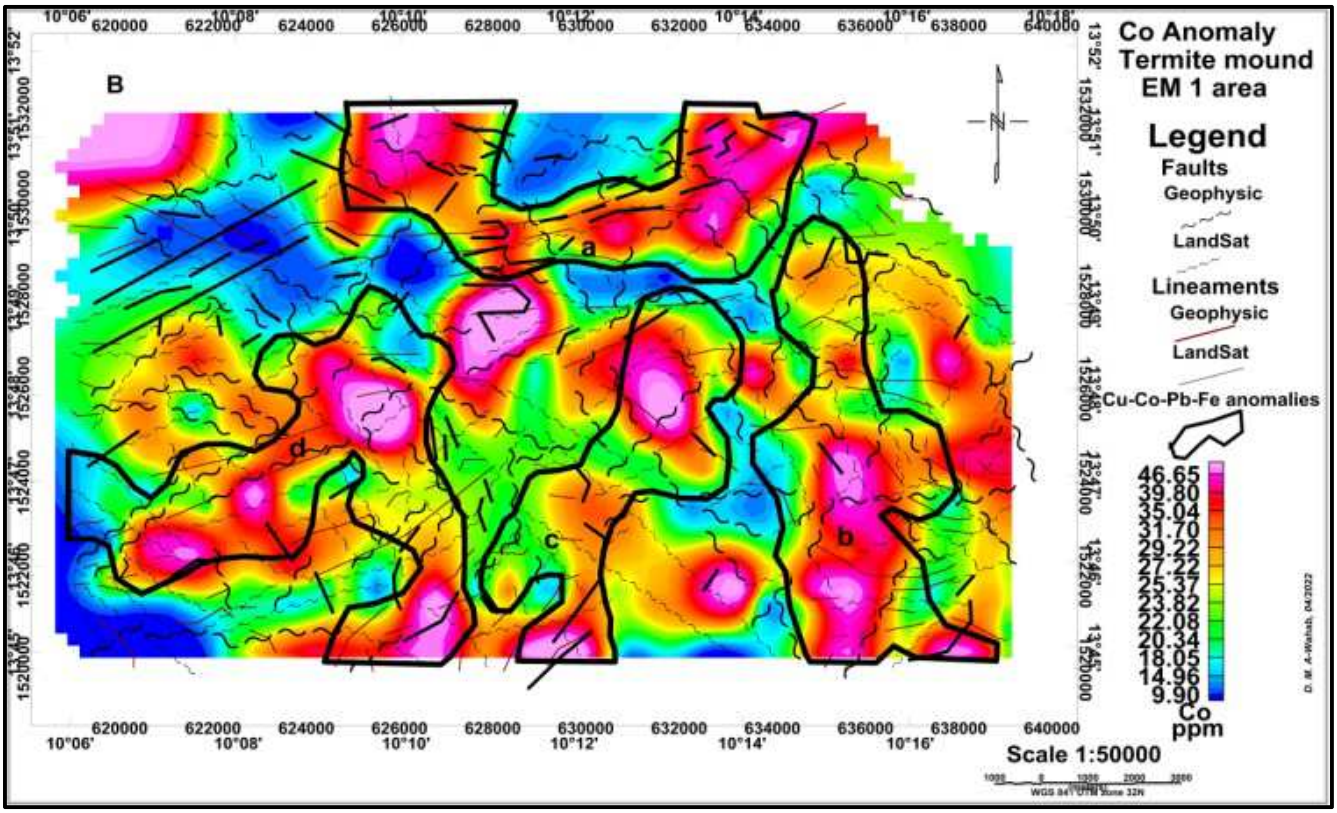

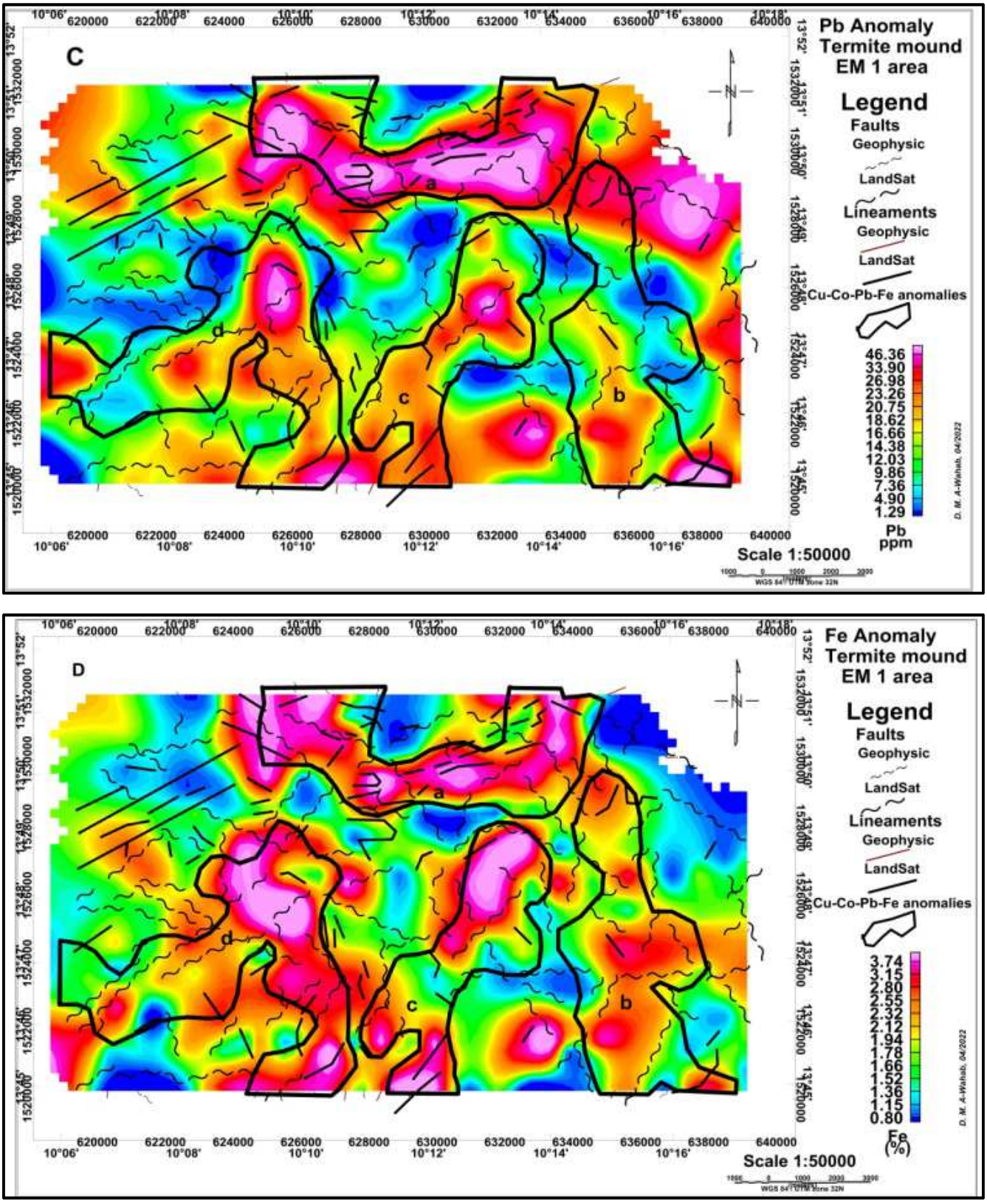

Figure 15. *Geochemical anomaly maps of the DMP, Cu (A), Co (B), Pb (C), Fe (D),*

5. Conclusions

The monovariate statistics, based on the different calculated parameters, have shown the interest of the results of this geochemical survey of termite mounds. Indeed, several grades of these mineral substances are higher than the Clark [33] but also than the anomalous threshold determined

by both the statistics and the cumulative frequency curves (Figure 3).

Multivariate statistics have allowed highlighting minerals with affinities, therefore polymetallic anomalies which grades vary in the same manner and others with grades that vary inversely.

The interpretation of satellite imageries and the analysis of high resolution geophysical data allowed specifying the structural context of these various anomalies. The faults orientations and also their spatial arrangement have been established. Some faults and lineaments interpreted by geophysics coincide with those interpreted from satellite imagery. Some of these anomalies are characterized by the presence of fault zones, conductive zones, potassium zones and a strong magnetic anomaly.

The geochemical anomaly maps of the fourteen mineral analyzed shown the location of the different anomalous zone for each of them. The cartographic coincidence of the anomalous zone of some of them highlights their correlation, which was confirmed by the factor analysis. The Termit mound geochemistry anomalous zones as well as the potassium anomalies don't seem to be associated to a particular lithology, according to the existing geological map of EM_1 area, but seem to be controlled by fault zones.

References

[1] ADAMA ZALEE, YOUSSOUF KOUSSOUBE contribution of soil geochemistry in the recognition of gold potentialities in lateritic cuirass context. Case of Foutouri in Burkina Faso University Ouaga 1 Pr Joseph KI-ZERBO Serie C, vol. 014, Juily 2018 ISSN: 2424-7545.

[2] ALAIN BLOT, (1998-2002), Methodology of mining prospecting in a lateritic environment and diversification of resources, Program, ORSTOM (lRD) - University of Ouagadougou – BUMlGEB.

[3] ARRUD J. R, YURMANI J., WACKERMANN J. I., (1979-1960), Geochemical data on copper, lead and zinc in Precambrian sediments of the Rio Ribeira de Iguape Basin (southeastern Brazil) and in their superficial mantle, Cah. O. R. S. T. O. M., Geol., vol. XI, II 1 43, 54p.

[4] BIRON S., MAI MANGA B., (1984-1986), Standard and methodology for geological mapping in Niger. CIDA and Ministry of Mines and Energy. Niamey, Niger.

[5] BLACK R. (1962), Draft on the younger granites of the Zinder-Gouré region. Report B. R. G. M, Dakar, Annexes.

[6] BLACK R. (1963), Note on the ring complexes of Tchouni-Zarnuski and Goure. Bull. B. R. G. M, FR., n°1.

[7] CHUDEAU R. (1907) Note on the alkaline rocks of Central Africa. C.R. Acad. Science. FR., 145 p.

[8] CLAIRE D., (2013) Factor analysis and reliability analysis, University of Montreal, Department of sociology, course note, https://www.google.com/url?sa=t&rct=j&q=&esrc=s&source=web&cd=&cad=rja&uact=8&ved=2ahUKEwigovvdieX5AhXBt6QKHZppA8UQFnoECAYAQ&url=https%3A%2F%2Fwww.webdepot.umontreal.ca%2FEnseignement%2FSOCIO%2FIntranet%2FSOL6210%2Fpublic%2Fnotesdecours%2Fanalyse_factorielle.pdf&usg=AOvVaw1cqJOdXp_VjQHKcz_ZF1ct.

[9] CLAUDE B. (1992), Application of geostatistical techniques and multivariate analysis to the interpretation of regional geochemical records, Thesis, University of Quebec in Montreal.

[10] CLAUDE L. (1969) A simplified statistical treatment of geochemical data by graphical representation, Economic Geology 64 (5): 538–550 p.

[11] DION P., (1973), Rapport final Permis Zinder-Maradi. Essex Iron Company, Niamey P. 60.

[12] FAURE H., (1951) End of campaign report 1950-1951: Reconnaissance east of Zinder. dir. Min. A.O.F.

[13] GENTIL L., (1904), on the existence of alkaline rocks in central Africa. C.R. Acad. Science. Fr., 139 p.

[14] GOURNAY A, (2012). Multivariate statistical analysis. Institute of Mathematics, University of Neuchâtel Switzerland.

[15] GREIGERT J. et POUGNET R. (1967)., Essays of geological description of the Republic of Niger. Department of Mines and Geology of Niger. Pub. n°3 and Memoir B. R. G. M. n°48.

[16] JEAN-PIERRE L. (1996) Geochemical anomalies in stream sediments - La Tuque region – Government of Quebec, Ministry of Natural Resources, Mining Sector, MB 96-35.

[17] LACROIX A. (1905), on the alkaline granites of the territory of Zinder. C.R. Acad. Science. FR., 140 p.

[18] LAMBERT R. (1933). Geological observations in the region between Agadez and Zinder. C R. Acad. Science. Q1, 489p.

[19] MATSCHULLAT J. 7 R. Ottenstein 7 C. Reimann, Geochemical background – can we calculate it?, Interdisciplinary Environmental Research Centre, Freiberg University of Mining and Technology, Brennhausgasse 14, D-09599 Freiberg, Saxony, Germany e-mail: matschullat@ioez.tu-freiberg.de, Environmental Geology 39 (9) July 2000.

[20] MIGNON R., (1970a), Explanatory note on the geological map of Damagaram-Mounio and South Maradi, at the scale 1/200,000. Ministry of Public Works, Transport, Mines and Urban Planning, Republic of Niger.

[21] MIGNON R., (1970b), Geological study and prospecting of Damagaram-Mounio and southern Maradi 68 ABI 006 NIA.

[22] MIGNON R., (1970b), Geological study and Prospecting of Damagaram-Mounio and South Maradi. Rap. B.R.G.M., 70 ABI 001, NIA.

[23] PRDSM, Niger Mining Sector Strengthening and Diversification Program, Mag/Spectro, Mag/EM airborne geophysical surveys in Aïr, Damagaram-Mounio and South Maradi. Ministry of Mines and Industrial Development, 2004-2010, 55 p.

[24] PROJET PAMM, (1998-2002). Support project to the Ministry of Mines and Energy of Niger, geological mapping and geochemical prospecting in South Maradi and Damagaram-Mounio.

[25] RAKOTONDRAMANO H., RAZAFINDRAKOTO B., FARASOA J., RASOLOMANANA M, (2021) Analysis of geochemical data by multivariate statistical methods, case of mining exploration in the North-West of Madagascar, University of Antananarivo, Institute and Observatory of Geophysics of Antananarivo, http://biblio.univ-antananarivo.mg.

[26] REIMANN C. PETER F., ROBERT G., (2002), Factor analysis applied to regional geochemical data: problems and possibilities, Applied Geochemistry, Volume 17, Issue 3, March 2002, pp 185-206.

[27] ROQUIN C., Ph. FREYSSINET, A. NOVIKOFF, Y. TARDY, Geochemistry of termite mounds and soils on cuirass: application to geochemical prospecting for gold in West Africa, Revue du BRGM - 1990/1991, pp 124-125.

[28] SURYA PRAKASH RAO K and S V RAJU, Geochemical analyses of termite mounds as a prospecting tool for tin deposits in Bastar, MP--a preliminary study, Indian Acad. Sci. (Earth Planet. Sci.), Vol. 93, No. 2, July 1984, pp. 141-148.

[29] SYLVAIN T. (2007), Identification of geochemical domains from regional lake-bottom sediment surveys, PROJECT 2004-09, Mining Exploration Research Consortium.

[30] TABACHNIK LINDA S. BARBARA G.; FIDELL. (2012): Using multivariate statistics. Harper and Row, New York. 983 p.

[31] TANGUAY M., BERARD J., (1973), Geological photo survey of Damagaram-Mounio and Tafidet Ditch. CIDA, 120p.

[32] THÉODORE Y., OLIVIER F., YEI OGA M-S., VINCENT A. (2012), Extraction of structural lineaments from satellite images and estimation of induced biases, in a metamorphosed Precambrian basement environment. Remote sensing, Editions contemporaries archives/ GB scientific editions / Gordon and Breach Scientific Publishers, 10 (4), pp. 161-178, hal-01948904.

[33] WILLIAM M. HAYNES, CRC Handbook of Chemistry and Physics, vol. 97, CRC Press/Taylor and FRANCIS, 2016, (ISBN 1498754287), «Abundance of elements in the Earth's crust and in the sea», p. 2652.